Discrete Algebraic Reconstruction Algorithm (DART)

Dimitrios Ieronymakis (s3372804), Maria Ieronymaki (s3374831)

***Abstract*—The main focus of Discrete Tomography is the reconstruction of images from a limited amount of projections. Some very common reconstruction algorithms are based on algebraic reconstruction techniques (ART). These methods model the reconstruction problem as an iterative optimization of a large system of linear equations. An interesting advantage of these methods is that they allow us to incorporate prior knowledge in the reconstruction process, fairly easily. In this paper, we will focus on the *Discrete Algebraic Reconstruction Technique* (DART), which extends common ART methods, by incorporating prior knowledge of the gray values in the reconstruction mechanism. As we will see, DART is capable of achieving better reconstructions than other similar algorithms, while also being more robust with respect to projections and angular range.**

***Index Terms*—DART, discrete tomography, reconstruction algorithm, phantom generation, projections, prior knowledge.**

I. Introduction

AMong several non-invasive imaging techniques, computational tomography is distinguished and popularly applied in the medical field for diagnostic purposes. Tomography is a technique that deals with the problem of reconstructing a sliced image of the respective object. The foundation of this technique lies on the so-called projections and the number of angles considered during the reconstruction process.

Nowadays, in addition to the classic Filtered Back Projection methods that are still very commonly used, several algebraic reconstruction techniques (ART) exist, which iteratively reconstruct the image based on a large system of linear equations. Furthermore, ART methods exploit the prior knowledge regarding the object, for instance, features like texture and material which could be known in advance. As a consequence, exploiting a certain prior knowledge during reconstruction, can lead to a more precise representation, while also using fewer projections and therefore, dealing with a less laborious process, in terms of time.

This paper aims to reconstruct both binary and gray-scale images, by assuming that each gray layer corresponds to a different material/depth of the object. As aforementioned, several algebraic reconstruction methods have been proposed so far that opt to solve discrete tomography problems. In our case, we focus on the implementation and evaluation of a technique called Discrete Algebraic Reconstruction Technique (DART), which alternates between "continuous" update steps and "discretization" steps, where the prior knowledge of the grey levels in the image is incorporated. The reconstruction of the image is considered as an array of real-valued unknowns that we want to identify by solving a large system of linear equations.

The outline of this paper is as follows. Section II, is dedicated to the detailed description of the DART algorithm, while in Section III, the phantoms utilized as test data are shown together with the experimental setup chosen in respect of the hyperparameter tuning conducted. Section IV, reports on the thoroughly selected experiments in order to evaluate the validity and the robustness of the DART algorithm by analyzing for instance, the impact of fundamental parameters' variation, such as the number of projections on the performance. Section V, concludes the report including assumptions on the conducted study and future work.

II. Method

DART is a reconstruction algorithm that alternates between continuous and discrete reconstruction steps. For the discrete step a segmentation operation can be used, while for the continuous step any algebraic reconstruction technique such as ART, SART and SIRT can be selected. In general, a DART iteration can be broken down in three main steps:

1) computing the $segmented$ image, resulting in an image with only the gray values defined a priori.
2) calculating the $free\ pixels\ U^{(t)}$ and $fixed\ pixels\ F^t$.
3) performing ART, on the free pixels.

These steps are explained in more detail in the following subsections. In Algorithm 1 the pseudocode of the algorithm is depicted. A more detailed explanation regarding the various steps described below can be found in the reference publication [1]. A step by step representation of the DART algorithm can be found in Figure 1, where the intermediate operations of 1 DART iteration, such us the segmentation in Figure 1(c) and the boundary pixels in Figure 1(d), can be observed.

A. Segmentation

In order to segment the reconstructed image into an image $s^{(t)}$, of only the gray levels R = $\{\rho_1, ..., \rho_l\}$, we calculate the intensity thresholds that denotes the set of intensities, which will be substituted by the gray level ρ_i, as such:

$$\tau_i = \frac{\rho_i + \rho_{i+1}}{2}$$

The thresholding function can be therefore indicated as following:

$$r(v) = \begin{cases} \rho_1, & (v < \tau_1) \\ \rho_2, & (\tau_1 < v < \tau_2) \\ ... & ... \\ ... & ... \\ \rho_l, & (\tau_{l-1} \leq v) \end{cases}$$

where, v expresses the pixel intensity (gray value of considered pixel) and $r(v)$ represents the resulting segmented image.

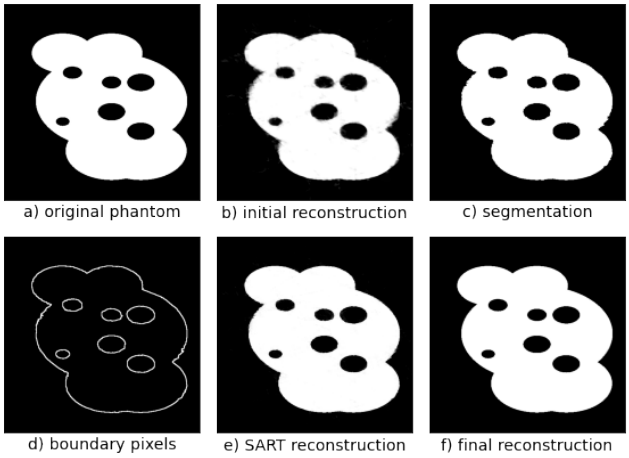

Fig. 1. Representation of the various steps used in the DART algorithm, applied on the Cloud phantom 2 presented in Section III: Initial reconstruction, Segmentation, Boundary pixels, SART reconstructions and final result

B. Calculation of free pixels

In the ARM step, DART updates only a subset of pixels, denoted as $free\ pixels\ U^{(t)}$. The $free\ pixels\ U^{(t)}$ are computed by calculating the set of $boundary\ pixels\ B^{(t)}$ from the segmented image $s^{(t)}$ and subsequently augmenting it with non-boundary pixels which are sampled randomly with probability $1-p$ from the previous reconstruction. To determine the boundary pixels $B^{(t)}$, the neighborhood of a pixel i is defined as $N(i) = \{1, ..., n\}$. In our specific case, where 2D phantoms are considered, the neighborhood of the pixel i corresponds to the 8 pixels that surround it. A pixel $s_i^{(t)}$ is therefore defined as boundary pixel if $s_i^{(t)} \neq s_j^{(t)}$ for any $j \in N(i)$.
To augment the set of free pixels we introduce a $fix\ probability\ 0 < p \leq 1$, which represents the probability of a pixel to not be included in $U^{(t)}$, but be considered as a $fixed\ pixel\ F^{(t)}$. Thus, the probability of a pixel to be considered a free pixel is $1-p$.

C. ARM on the fixed pixels

As far as the continuous reconstruction step is concerned, any algebraic reconstruction algorithm can be used. As stated in the reference DART publication, the application of the reconstruction algorithm on the $free\ pixels\ U^{(t)}$, yields better results if the correct values have been assigned to the $fixed\ pixels\ F^{(t)}$. The reconstruction algorithm suggested in the original paper [1] is SART with a randomized updating scheme. A detailed original publication of SART can be found in [2]. However, other reconstruction algorithms can be used such as SIRT [6] and FBP [7].

In order to apply the update to the free pixels only, a decomposition of the following forward projection problem is needed, in order to extract the free pixels' sinogram as follows:

$$Ax = sinogram$$

$$A(x_{free} + x_{fixed}) = sinogram$$

where:
- A is the projection matrix
- x represents the current reconstruction
- x_{free} denotes the current reconstruction with all the fixed pixels set to 0 .
- x_{fixed} indicates the current reconstruction with the free pixels set to 0.

In addition, following the fact that $Ax_{free} = sinogram_{free}$ and $Ax_{fixed} = sinogram_{fixed}$, the calculation of the free pixels' sinogram is computed by substituting the above terms in the previous equation as below:

$$sinogram_{free} = sinogram - sinogram_{fixed}$$

D. Smoothing Operation

The smoothing operation is used with the aim of normalizing the possibly high fluctuations in the values of the reconstructed free pixels $U^{(t)}$. According to the original DART paper implementation [1], following the ARM step, a Gaussian smoothing filter of radius 1 is applied to the free pixels.

E. Termination criterion

Since DART does not have a convergence theory to back up the algorithm, is not possible to specify an exact condition for which the algorithm should terminate. Thus, the algorithm's termination is determined by the number of iterations we want to perform, or the $total\ projection\ error$ defined as:

$$E(x) = ||Wx - p||_2$$

with $E : \mathbb{R}^n \to \mathbb{R}$
where:
$W \in \mathbb{R}_{\leq 0}^{m \times n}$: is projection matrix
x : is the reconstructed image
p : is the vector of measured measured projection data.

III. Experimental setup

A. Phantoms and measurements

The algorithm's performance, was evaluated by creating phantom images. The four families of pixel-based phantoms used are represented on a pixel grid in Figure 2, where each row corresponds to the following phantom families respectively: *CLoud*, *Paw*, *Semilunar* and *Alien*. The first two families are binary while, the Semilunar and Alien families have multiple gray values.

To create different phantoms for each family, a certain noise was applied to modify the original image, by removing, adding, moving or resizing objects that compose it. Each generator is capable of creating n images (in our case $n = 3$) of both 256x256 and 512x512 dimensions. However, since 512x512 is an image size that is also common in practical CT applications, the latter was specifically used in the simulation experiments. As for the reconstructions, the same image size as that of the created phantoms was used.

Algorithm 1: DART pseudocode

Input : $iters$ = dart iterations
η = max error
g_l = gray values
p_free = free pixels prob
$proj$ = projections
ARM_alg = ART algorithm
rec_iters = ART iterations

Termination: The algorithm terminates when:
- we perform $iters$ number of iterations
- the reconstruction error is lower than η

$x^{(0)}$ = initial reconstruction with ARM_alg
t = 0
x_err = + ∞
while $t < iters$ ***and*** $x\_err > \eta$ **do**
  $t = t + 1$
  $s^{(t)}$ = segmented $x^{(t-1)}$;
  $U^{(t)}$ = free pixels of $s^{(t)}$ defined by p_free
  $F^{(t)}$ = fixed pixels of $s^{(t)}$
  $y_i^{(t)}$ = $s_i^{(t)}$ if pixel i $\in$F$^{(t)}$ else $x_i^{(t-1)}$
  $x^{(t)}$ = $ARM\_alg(y^{(t)})$ without updating the fixed pixels
  $x_i^{(t)}$ = $y_i^{(t)}$ if pixel i in $F^{(t)}$
  if t < iters - 1:
    $x_i^{(t)}$ =smoothing $x_i^{(t)}$ if pixel i in $U^{(t)}$
end

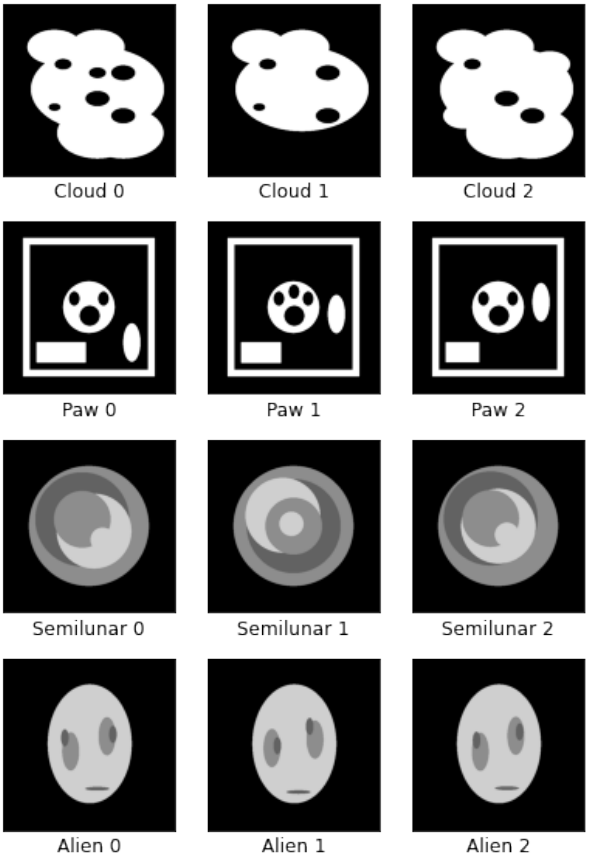

Fig. 2. Representation of the four phantom families generated. We will refer to the first row of phantoms as $Cloud$ phantoms, row 2 as Paw phantoms, row 3 as $Semilunar$ phantoms and finally, row 4 as $Alien$ phantoms. For each generation, a certain noise has been added in order to yield a slightly different phantom.

In order to sample measurements (in the form of projections) from the images, a parallel projection geometry was used with 512 detector values. On the contrary, the number of projections and the angle range were varied for each specific experiment.

To create the projections and implement all the algorithms, the $ASTRA\ toolbox$ was used. To learn more about this tomography library you can refer to the following documents in [3], [4] and [5].

B. Tuning and Parameters

Since the number of iterations of both DART and SART algorithm and the value of the fix probability play a fundamental role in the quality of the reconstruction, before conducting the necessary experiments for the evaluation of the reconstruction performance, a preliminary tuning experiment was conducted. It is important to underline the fact that the tuning experiments were run one time and only for limited phantoms. However, they were more than sufficient to determine the appropriate values for the parameters used in the following experiments. As a metric to compare our results throughout all the experiments, the $Mean\ Absolute\ Pixel\ Error$ metric was used. The metric is defined as the mean absolute distance of the value of the pixels between the reconstructed image and the original phantom.

The initial tests were performed on the binary phantoms Cloud 0, Paw 1 and on the grey-scale Semilunar 1. The experiments' results were useful to verify that the parameters performed equally well not only on simple phantoms, but also on the ones of greater complexity. The final parameters' selection for the main experiments was based on the combination of the Mean absolute error metric and the time necessary to obtain the reconstruction. The following tuning experiments were run with 50 projections and 180°angle range for the measurements. Table I shows a subgroup of the parameters tested and the results obtained from the tuning experiments.

Firstly, we experimented with the parameters used in the reference paper [1]: 200 DART iterations, 3 ART steps of SART, per DART iteration and a p_{fixed} value of 0.85. As we can deduce from the table, as far as the Cloud phantom is concerned, this setting yielded a mean absolute error of 2.2, and the time necessary to reconstruct the image was around 5 minutes. An interesting finding was that by reducing the number of DART iterations to 100 and simultaneously increasing the reconstruction iterations of SART to 10, resulted in obtaining a slightly lower mean absolute error of 2.13 in

DART iter	SART iter	p	Pixel error	Time
Cloud phantom 0				
200	3	0.85	2.2	5 min 10s
100	10	0.85	2.13	2 min 35s
50	100	0.85	1.11	1 min 19s
50	100	0.9	0.88	1 min 19 s
10	1000	0.9	0.06	19s
Semilunar phantom 1				
200	3	0.85	1.24	5 min 11s
100	10	0.85	1.04	2 min 34s
50	100	0.85	0.6	1 min 19s
50	100	0.9	0.52	1 min 20s
10	1000	0.9	0.32	19s
Paw phantom 1				
50	100	0.85	1.93	1 min 20s
10	1000	0.9	0.63	19s
50	1000	0.9	0.62	1 min 35s

TABLE I
PARAMETER TUNING RESULTS BASED ON DIFFERENT VALUES FOR DART AND SART ITERATIONS AND FIX PROBABILITY, ON PHANTOMS CLOUD 1, SEMILUNAR 1 AND PAW 1. THE PARAMETERS' SELECTION WAS BASED ON THE MEAN ABSOLUTE ERROR METRIC AND THE TIME NECESSARY TO OBTAIN THE RECONSTRUCTION.

half of the time needed when using the previous settings. By taking advantage of the information retrieved from the initial and subsequent experiments on the Cloud 0 phantom, the analysis continued on the Semilunar 1 and the Paw 1 phantoms by setting the DART iterations to 50 and 10, and the SART iterations to 100 or 1000. In the Semilunar phantom we again notice that the configuration with only 10 DART iterations, yielded the best (lowest mean absolute pixel error) and fasted reconstruction. Finally, in the Paw phantom we run the best configurations found in the previous experiments, where a pixel error of 0.62 was achieved. However, since the reconstruction error did not improve drastically when using 10 or 50 DART iterations, the configuration parameters chosen for the main experiments, were the following:

- DART iterations ($DART_{iterations}$): 10
- p_{fixed}: 0.9
- ART steps for DART ($DART\_ART_{iters}$): 1000
- compared algorithms iterations: 10.000

For experiments where a different number of DART iterations was used, (usually in the qualitative experiments), the number of iterations for the compared algorithms was kept proportionate to the total amount ART steps done in DART as $DART_{iterations} \cdot DART\_ART_{iters}$.

IV. EXPERIMENTS AND RESULTS

This section reports the experiments conducted in order to evaluate the reconstruction performance of the DART algorithm, compared to the algorithms aforementioned.

All the experiments were run for each phantom and results were averaged for each phantom family in the following figures and plots referenced. The transparent areas around the curves represent the standard deviation of the algorithm for the three phantoms of each family. In addition, since it was noticed that SART and SIRT achieve usually better reconstructions when passed through the same segmentation function used in DART, the qualitative reconstruction of those algorithms has also been reported in the document.

A. Varying the Number of Projections

This experiment was performed in order to see how the quality of the reconstruction and the mean absolute pixel error varied with respect to the number of projections considered. For the experiment, the number of projections was increased from 2 to 20 with a 2 projection increment between each step. Results have been reported in Figure 3. As we can notice from Figure 3, the pixel error decreases as the number of projections increases, for all algorithms. The results show that, for the Paw phantom, DART is able to achieve considerably better reconstructions than its competitors, with only 8 to 10 projections. On the contrary, regarding the Alien and Semilunar phantoms, DART is consistently achieving the best reconstructions for every number of projections.

In Figure 4, a qualitative representation of the Paw phantom 0 reconstructions of different algorithms, can be observed for 8 projections. It is interesting to notice how in the example, SART is able to achieve a better reconstruction error when a final segmentation is applied, although the reconstruction is not as precise as DART's. This may be due to the metric chosen, which may not be the most informative regarding the quality of the image, however, it is still considered an appropriate indicator for the general algorithm's performance. Nonetheless, segmenting the DART reconstruction as a last step, would probably yield even better results.

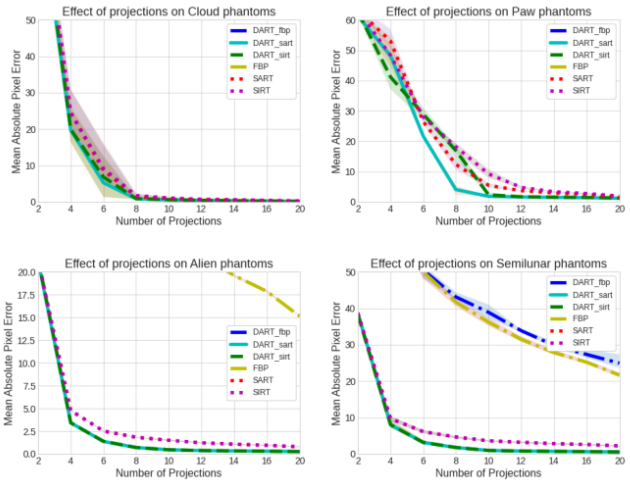

Fig. 3. The graphs shows the mean absolute pixel error as a function of the number of projections, averaged over each phantom family. The angle range used to sample measurements was of 180°. FBP and DART with FBP are not visible in some of the plots since their errors diverged to very high values.

B. Varying the Number of Angles

As stated in the original paper in DART, in many industrial applications the angle range used to sample projections is limited. Therefore, we benchmarked DARTs' performance as a function of the angle range. The experiments carried out are depicted in Figure 5, where the angle range is varied from 10°to 180°. The various graphs show that DART converges similarly to the other algorithms and in specific cases even achieve better reconstructions for very limited angle ranges,

Fig. 4. The images represent the reconstructions of the various algorithms under the assumption of low number of projection. The reconstructions are based on 8 projections and an angle range of 180 °. DART was run for 50 iterations, with 1000 ART iterations and p_{fixed} = 0.99, while, the compared algorithms were run for 50.000 iterations. The mean absolute pixel errors for each reconstruction are the following: (b) DART error: 1.59, (c) SART error: 8.84, (d) SART segmented error: 1.33, (e) SIRT error: 13.42, (f) SIRT segmented error: 2.40 .

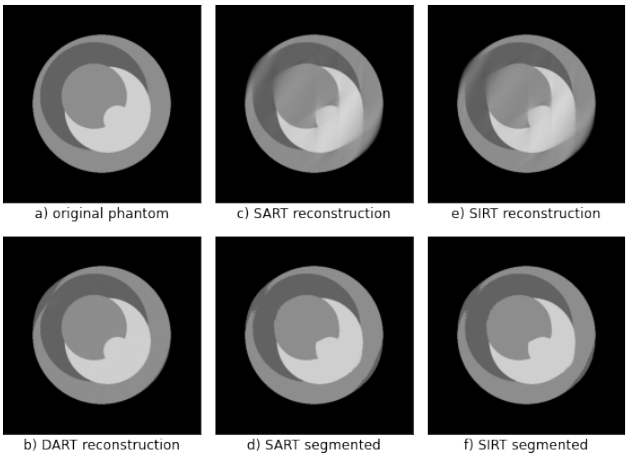

Fig. 6. Comparison of DART, SART and SIRT algorithms on the Semilunar phantom 1, for 50 projections and an angular range of 120°. All the algorithms were run for a total of 50.000 iterations. The compared SART and SIRT algorithms are reported both with their original reconstruction and with the DART segmentation applied at the end. The mean absolute pixel errors for each reconstruction are the following: (b) DART error: 0.88, (c) SART error: 2.14, (d) SART with segmentation error: 1.37, (e) SIRT error: 2.17, (f) SIRT with segmentation error: 1.4 .

compared to SART and SIRT. This phenomenon is especially visible on the Cloud phantoms' graph, where DART is able to achieve acceptable reconstructions for angle ranges between 50°and 80°. On the other hand, by observing the Alien and Semilunar phantoms' plot, we see that DART is consistently delivering better reconstructions than its competitors.

In Figure 6, a qualitative representation of the reconstructions obtained with different algorithms is given, for the Semilunar phantom 0, sampled with an angle range of 120°and 50 projections. All the segmented reconstructions are able to achieve results similar to DART, however we believe that DARTs' reconstruction is still superior among the others.

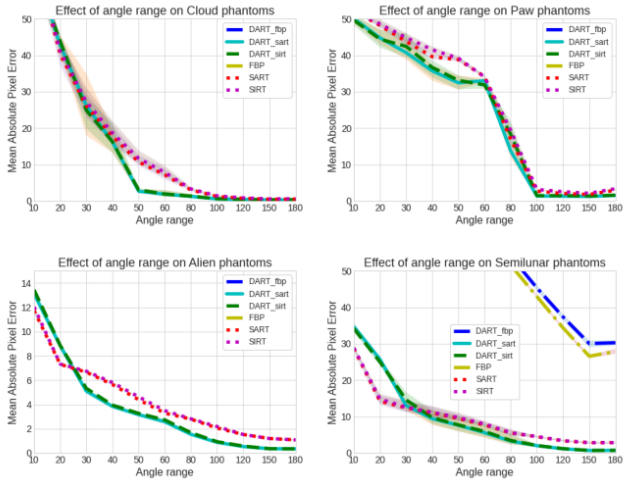

Fig. 5. The graphs show the mean absolute pixel error as a function of the angle range, averaged over each phantom family. The number of projections was kept constant to 14 projections per measurement. FBP and DART with FBP are not visible in some of the plots since their errors diverged to very high values.

C. Varying the Number of Projections and Angles simultaneously

In order to see the combined effect of the number of projections and angle range on the reconstruction quality, an experiment was carried out where the two were varied simultaneously. Results of this experiment are displayed in Figure 7. The results reinforce what the previous two experiments already displayed. DART is able to converge similarly to its competitors, while in the case of the Alien and Semilunar phantoms, achieves better and more robust overall reconstructions.

In Figure 8, a comparison of the various reconstructions is shown as a qualitative example of the reconstruction performance, under the assumption of a low number of projections, for the Alien 0 phantom. The results are fairly visible, with SART and SIRT reconstructions not being as sharp as DARTs', even when the segmentation is applied.

D. Noisy Projection Data

The following experiment, together with the one reported in IV-E, was carried out in order to simulate DARTs' performance under real-world conditions. Since real-world data usually contains a certain amount of experimental noise, it was necessary to evaluate DART's performance in case of noisy projection data. In the experiment, the Poisson noise in the original measurements was increased from 0% to 17%.

The results obtained show as expected that all algorithms' errors increase linearly with higher Poisson noise in the projections. An intriguing observation however, can be made about the SART based algorithms, which seem to deviate more than the SIRT configurations for higher values of noise. This may be associated to the nature and updating scheme of the two algorithms.

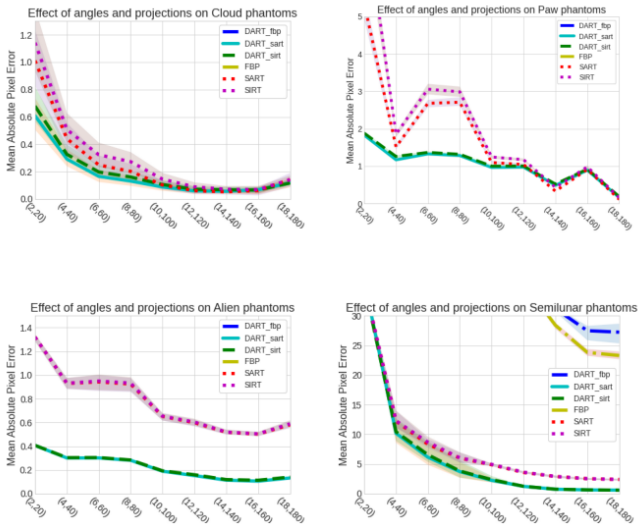

Fig. 7. Mean absolute pixel error as a function of the number of projections and angle range varied simultaneously. The number of projections was varied from 2 to 18, while the angle range from 20°to 180°.

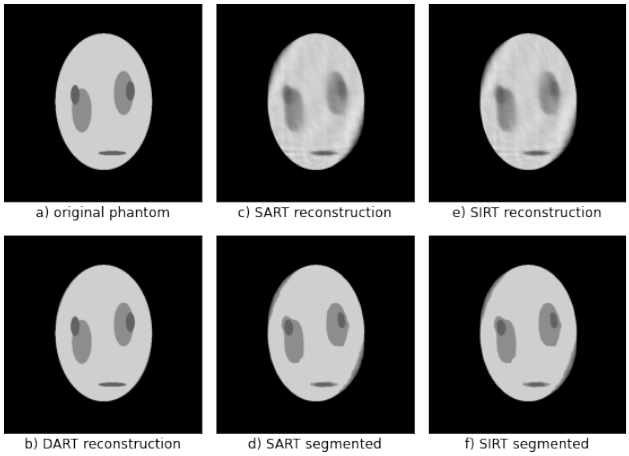

Fig. 8. Comparison of DART, SART and SIRT algorithms on the Alien phantom 2, for 12 projections and an angular range of 120°. All the algorithms were run for a total of 50.000 iterations. The compared SART and SIRT algorithms are reported both with their original reconstruction and with the DART segmentation applied at the end. The mean absolute pixel errors for each reconstruction are the following: (b) DART error: 0.42, (c) SART error: 2.84, (d) SART with segmentation error: 2.36, (e) SIRT error: 2.85, (f) SIRT with segmentation error: 2.38 .

E. Varying the Grey Levels

An additional experiment was conducted to determine whether the algorithm was sufficiently robust. By that means, since in practical applications the exact grey levels may not be known, it was unavoidable to evaluate whether the reconstructions quality obtained was equally satisfactory without assuming the gray levels in the phantoms to be perfectly known a priori. Three main experiments were run on this section, by sampling the gray value noise in different ways. In the first experiment, we tested the effect of the overestimation of the gray values, while, in the second one we tried to underestimate the gray values in the original phantom. Furthermore, a last experiment was conducted that combined the two approaches

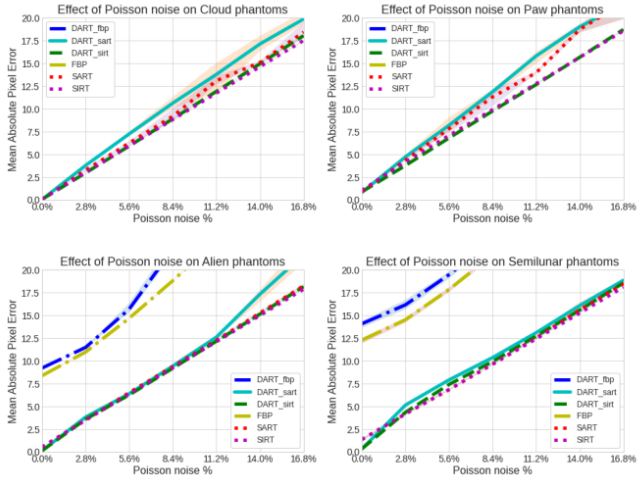

Fig. 9. Mean absolute pixel error as a function of the applied Poisson noise on projections. The experiment relied on measurements of 50 projections and an angular range of 180°.

aforementioned, where the sign of the noise was sampled randomly in order to have mixed, random overestimation and underestimation. Experiments were run with a gray level error varying from 2% to 40%, with 2% step increments. The results are visible in Figures 10, 11 and 12.

Some interesting observations can be made from the behaviour of the algorithm under various types of noise. Overestimating the values leads to a higher but more stable error in the reconstructions, compared to when underestimating them. In contrast, when dealing with underestimated values, the error increases almost linearly with the applied gray value estimated error. Finally, in Figure 12, where the results of the mixed approach experiment are depicted, the error becomes fairly unstable and in the case of the binary phantoms, the algorithm sometimes achieves acceptable reconstructions even with high estimation errors.

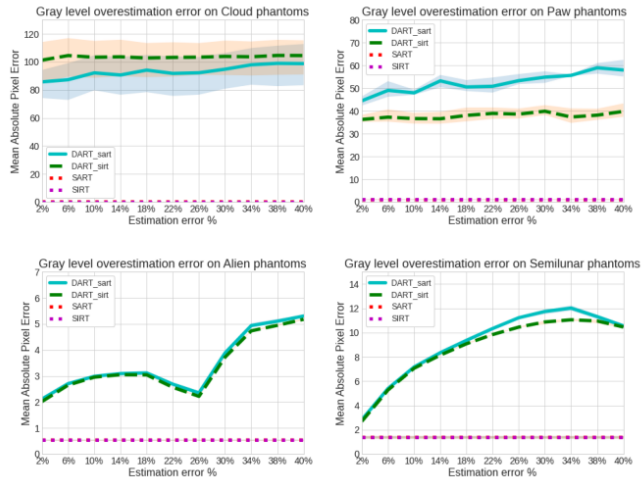

Fig. 10. Mean absolute pixel error as a function of the overestimated gray value error. The gray levels were overestimated from 2% to 40%, with 2% step increments. The experiment relied on measurements of 50 projections and an angular range of 180°.

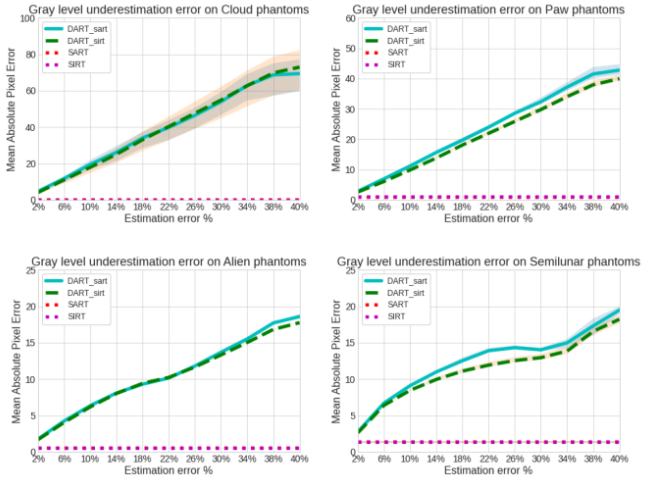

Fig. 11. Mean absolute pixel error as a function of the underestimated gray value error. The gray levels were overestimated from 2% to 40%, with 2% step increments. The experiment relied on measurements of 50 projections and an angular range of 180°.

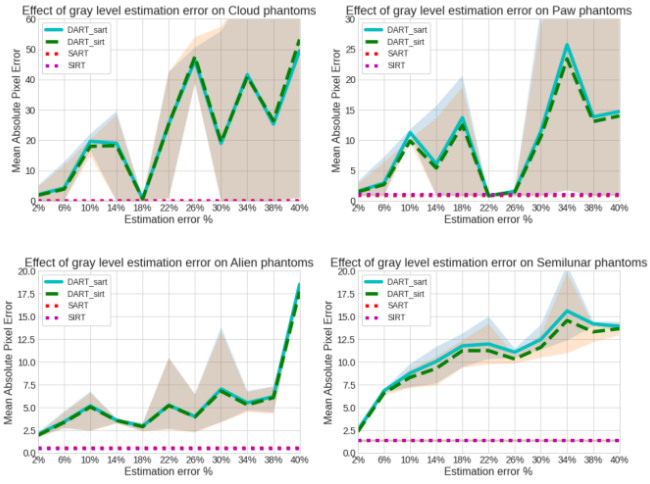

Fig. 12. Mean absolute pixel error as a function of the gray value estimation error for both overestimated and underestimated gray values. The gray levels were randomly overestimated or underestimated from 2% to 40%, with 2% step increments. The experiment relied on measurements of 50 projections and an angular range of 180°.

F. Varying the p_{fixed} value

One of the main hyperparameters of DART is definitely the p_{fixed} value that defines the probability of the fixed and free pixels. In this experiment we varied the value of p_{fixed} from 0.0 to 1.0. The results can be observed in Figure 13, where it can be noticed that the Mean Absolute Pixel Error decreases similarly for all phantoms, as the value of the p_{fixed} increases, reaching its minimum when the p_{fixed} value is equal to 1. The only exception is for the Semilunar phantoms, where the standard deviation of the error increases for higher p_{fixed} values.

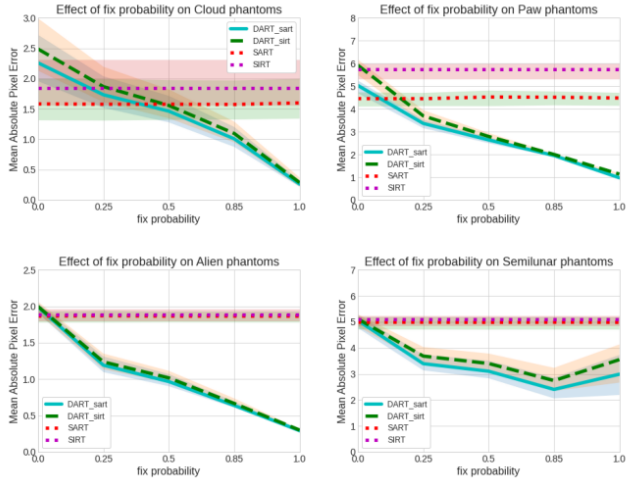

Fig. 13. Mean absolute pixel error as a function of the p_{fixed} probability. The experiment relies on 10 projections and an angular range of 120°. The p_{fixed} probability is varied from 0.0 to 1.0 .

V. Discussion and Conclusions

Overall, we can conclude that DART prevails over other algebraic reconstruction algorithms, such as SART, SIRT and FBP. DART tends to shine especially in applications with a low number of projections or limited angle range. As we saw from the quantitative experiments, DART can achieve better reconstructions than its competitors in the same number of reconstruction iterations.

Regarding the reconstruction time of DART, as we noticed from the tuning experiments in Section III, running DART for a lower amount of iterations with a higher number of the ART steps produces better reconstructions in a much lower run time. This could also be related to the nature of the phantoms, although it seems improbable.

Focusing now on the various configurations tested, it can be concluded that FBP and DART with FBP are not able to achieve equally satisfactory results compared to the configurations with SIRT and SART. In fact, the two configurations are rarely visible in our plots. SIRT and DART with SIRT were the most stable and returned the most consistent results. On the other hand, DART with the SART subrutine and SART itself achieve better results than the SIRT configurations, in some circumstances, as seen in the experiments in section IV-A for the Paw phantoms, and in the p_{fixed} experiments in section IV-F, for all phantoms. However, when affected with Poisson noise and Gray value estimation errors the SART configurations have a higher standard deviation in the error. This may be due to the random update scheme that SART utilizes.

Considering now the Poisson noise experiments, we observe that DART can be as robust as the compared reconstruction algorithms. Nevertheless, for high noise values ($\geq$ 3%), the error difference between the various algorithms can be considered negligible, since the reconstructions would not be acceptable in real life tomography applications.

Moreover, the gray value experiments' results were very interesting since the different behaviour for overestimation

and underestimation could imply that there is a possibility to deduce them when unknown. More experimentation with different phantoms would be required to develop a strategy to tune the gray values accordingly when we lack of prior knowledge.

The results on the p_{fixed} parameter (section IV-F) show that the best reconstructions for the majority of the phantoms were achieved with a p fixed value of 1. Since the free pixels are used to create new boundaries, it could be more effective in phantoms with many ”empty areas” inside, in the form of holes. Further experimentation could lead to a better understanding of the behaviour of the p value for phantoms with a more complex structure.

REFERENCES

[1] K. J. Batenburg and J. Sijbers, ”DART: A Practical Reconstruction Algorithm for Discrete Tomography,” in IEEE Transactions on Image Processing, vol. 20, no. 9, pp. 2542-2553, Sept. 2011, doi: 10.1109/TIP.2011.2131661.

[2] Andersen AH, Kak AC. Simultaneous algebraic reconstruction technique (SART): a superior implementation of the art algorithm. Ultrason Imaging. 1984 Jan;6(1):81-94. doi: 10.1177/016173468400600107. PMID: 6548059.

[3] W. van Aarle, W. J. Palenstijn, J. Cant, E. Janssens, F. Bleichrodt, A. Dabravolski, J. De Beenhouwer, K. J. Batenburg, and J. Sijbers, “Fast and Flexible X-ray Tomography Using the ASTRA Toolbox”, Optics Express, 24(22), 25129-25147, (2016), http://dx.doi.org/10.1364/OE.24.025129

[4] W. van Aarle, W. J. Palenstijn, J. De Beenhouwer, T. Altantzis, S. Bals, K. J. Batenburg, and J. Sijbers, “The ASTRA Toolbox: A platform for advanced algorithm development in electron tomography”, Ultramicroscopy, 157, 35–47, (2015), http://dx.doi.org/10.1016/j.ultramic.2015.05.002

[5] W. J. Palenstijn, K. J. Batenburg, and J. Sijbers, “Performance improvements for iterative electron tomography reconstruction using graphics processing units (GPUs)”, Journal of Structural Biology, vol. 176, issue 2, pp. 250-253, 2011, http://dx.doi.org/10.1016/j.jsb.2011.07.017

[6] Dilz, Roeland J. and Schröder, Lukas and Moriakov, Nikita and Sonke, Jan-Jakob and Teuwen, Jonas, “Learned SIRT for Cone Beam Computed Tomography Reconstruction”, arXiv, 2019, https://doi.org/10.48550/arxiv.1908.10715

[7] Özge Onur, T. (2021). An application of filtered back projection method for computed tomography images, International Review of Applied Sciences and Engineering, 12(2), 194-200. Retrieved Jun 15, 2022, from https://akjournals.com/view/journals/1848/12/2/article-p194.xml

M.I. developed the phantom generator, D.I. implemented the DART algorithm and conducted the experiments. Both authors discussed the results and contributed to the final manuscript.